Supplementary Information

Cu-based MOF-derived porous carbon with highly efficient photothermal conversion performance for solar steam evaporation

Guanyu Chen[1], Zipeng Jiang[2], Ang Li[1]*, Xiaohong Chen[1], Zhaokun Ma[1], Huaihe Song[1]*

1. State Key Laboratory of Chemical Resource Engineering, Beijing Key Laboratory of Electrochemical Process and Technology for Materials, Beijing University of Chemical Technology, Beijing, 100029, PR China.

2. Key Laboratory of Advanced Materials and Applied Technology for Qinghai Province, Qinghai University, Xining 810016, PR China.

*Corresponding Author: E-mail: songhh@mail.buct.edu.cn.(Huaihe Song),
li_ang@mail.buct.edu.cn(Ang Li)

SI.1 SEM images of samples with different pyrolysis temperature and CBC-T

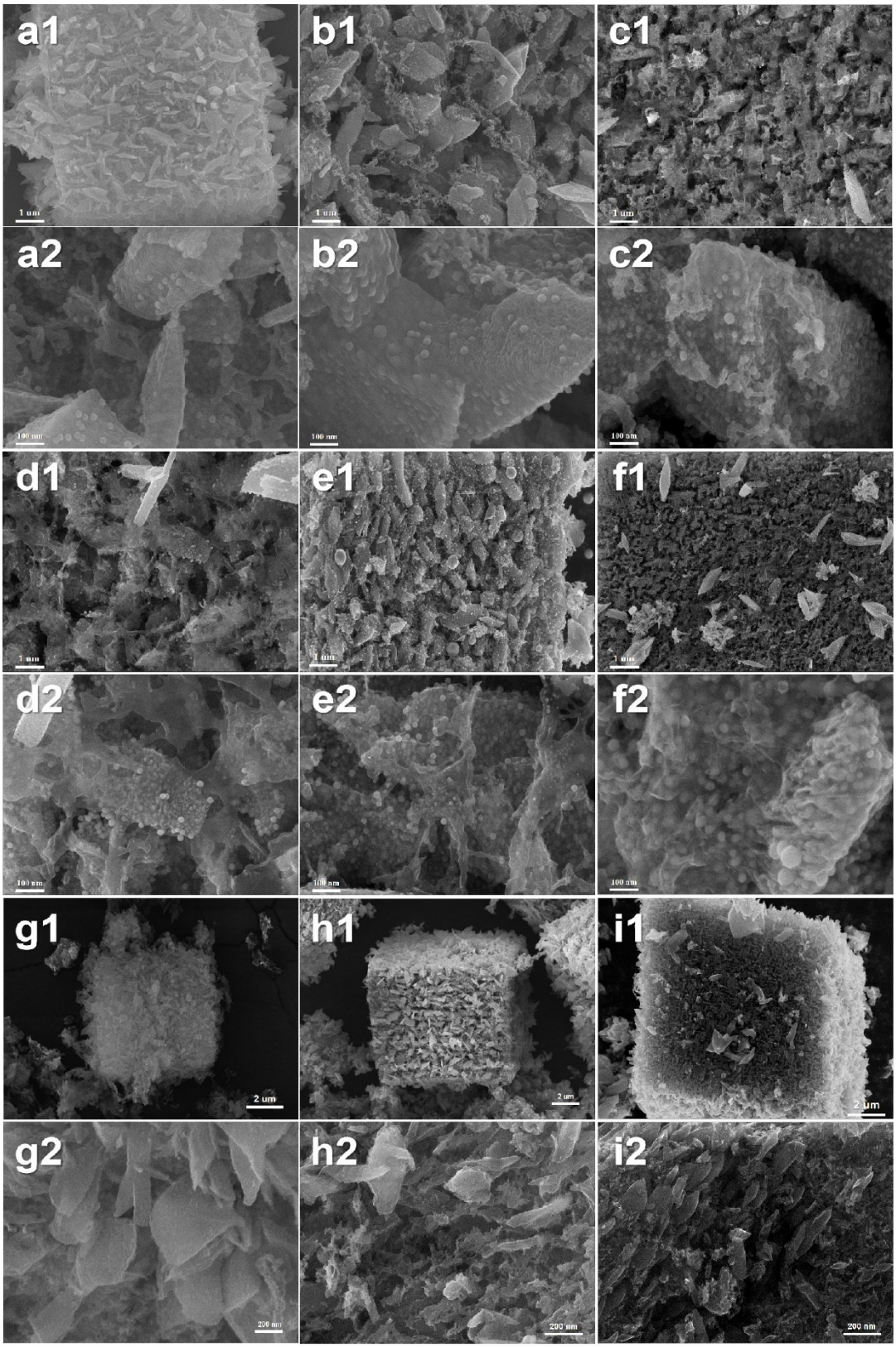

Figure S1 SEM images of Cu-BDC pyrolyzed at (a1& a2) 400℃, (b1&b2) 500℃, (c1&c2) 600℃, (d1&d2) 700℃, (e1&e2) 800℃ and (f1&f2) 900℃; The morphology of (g1&g2) CBC-400, (h1&h2) CBC-600, (i1&i2) CBC-800.

SI.2 SAED images of CBC-900

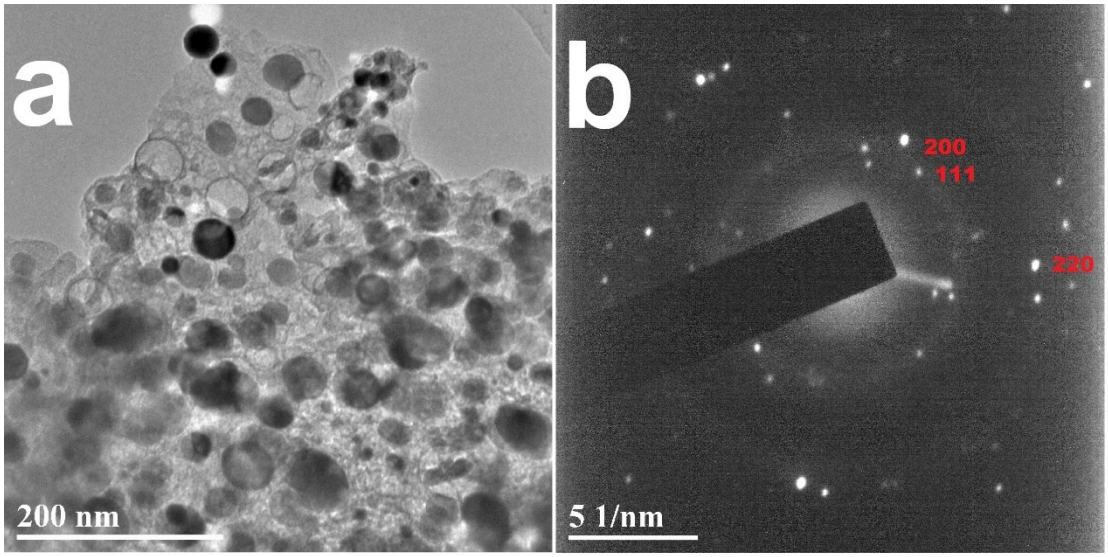

Figure S2. The HRTEM image of (a) CBC-900 without washed by ammonia and 6 M HCl and (b) the corresponding SAED image.

SI.3 Porous property characterization of CBC-T

Table S1. Structural parameters and the Thermal Conductivity of CBC-T samples.

Sample	[a]S_{BET} ($m^2\ g^{-1}$)	[b]S_{micro} ($m^2\ g^{-1}$)	[c]S_{meso} ($m^2\ g^{-1}$)	[d]V_{total} ($cm^3\ g^{-1}$)	[e]V_{micro} ($cm^3\ g^{-1}$)	[f]V_{meso} ($cm^3\ g^{-1}$)	Thermal Conductivity (W/mK)
CBC-400	718.9	153.9	565	1.027	0.064	0.963	0.035
CBC-500	453.8	199.3	254.5	0.62	0.09	0.51	0.035
CBC-600	462.3	198.1	264.2	0.599	0.099	0.5	0.037
CBC-700	439.7	128.5	311.3	0.522	0.076	0.348	0.041
CBC-800	396.1	119.6	276.5	0.565	0.059	0.419	0.05
CBC-900	201.4	45.4	155.97	0.29	0.022	0.229	0.052

a Specifific surface area calculated by BET method.

b Specifific surface area of micropores calculated by t-plot method.

c Specifific surface area of mesopores calculated by BJH method.

d Total pore volume.

e Volume of micropores.

f Volume of mesopores.

SI.4 Structure and composition of CBC-T and the samples pyrolyzed at 300 ℃ and Calculation of R value of CBC-T.

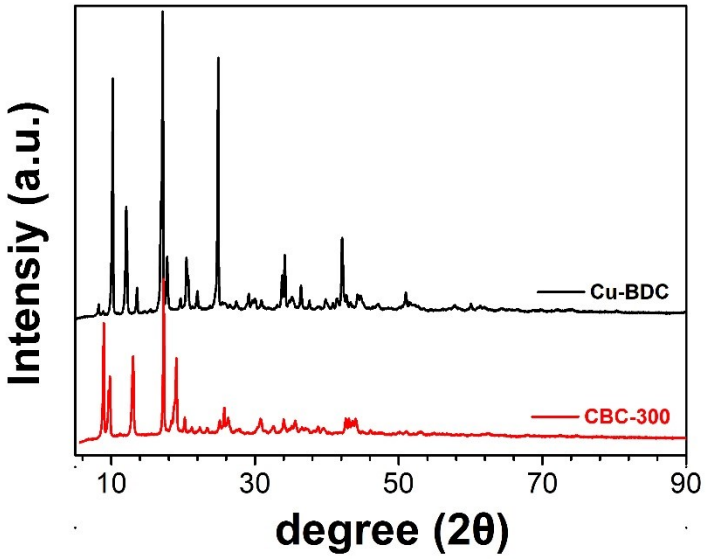

Figure S3. XRD image of CBC-300 and Cu-BDC.

With reference to the Figure S4, the background (A) is established by drawing a straight line connecting the data on either side of the peak. The peak height (B), is determined by drawing the line tangent to the linear background estimate, which intersects the (002) peak in a single point. R value is then taken to be B/A. We use this simple definition for quick and easy comparison of samples.

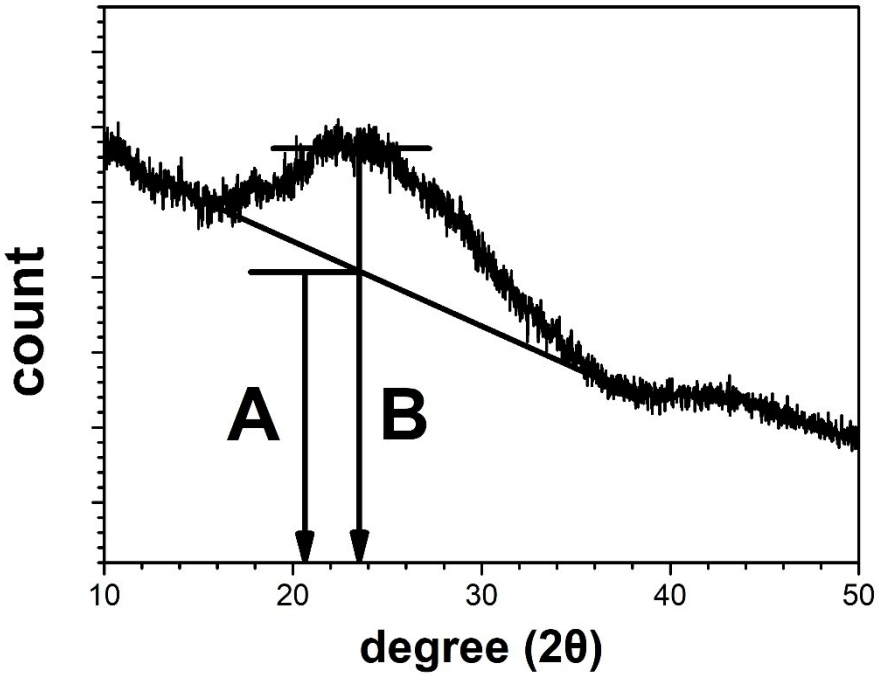

Figure S4. The empirical parameter R value is defined schematically.

SI.5 The TG image of Cu-BDC

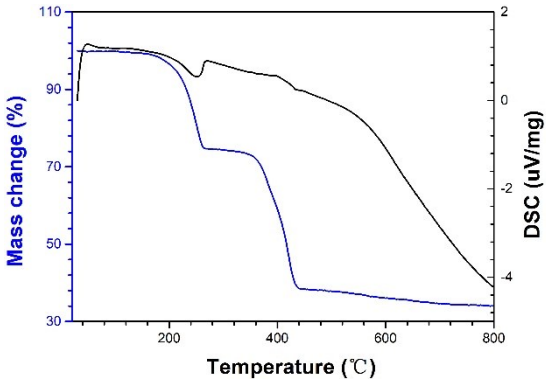

Figure S5. In situ characterization of evolution of molecular composition of the pyrolytic Cu-BDC by TG.

SI.6 The Raman and XPS spectra of CBC-T

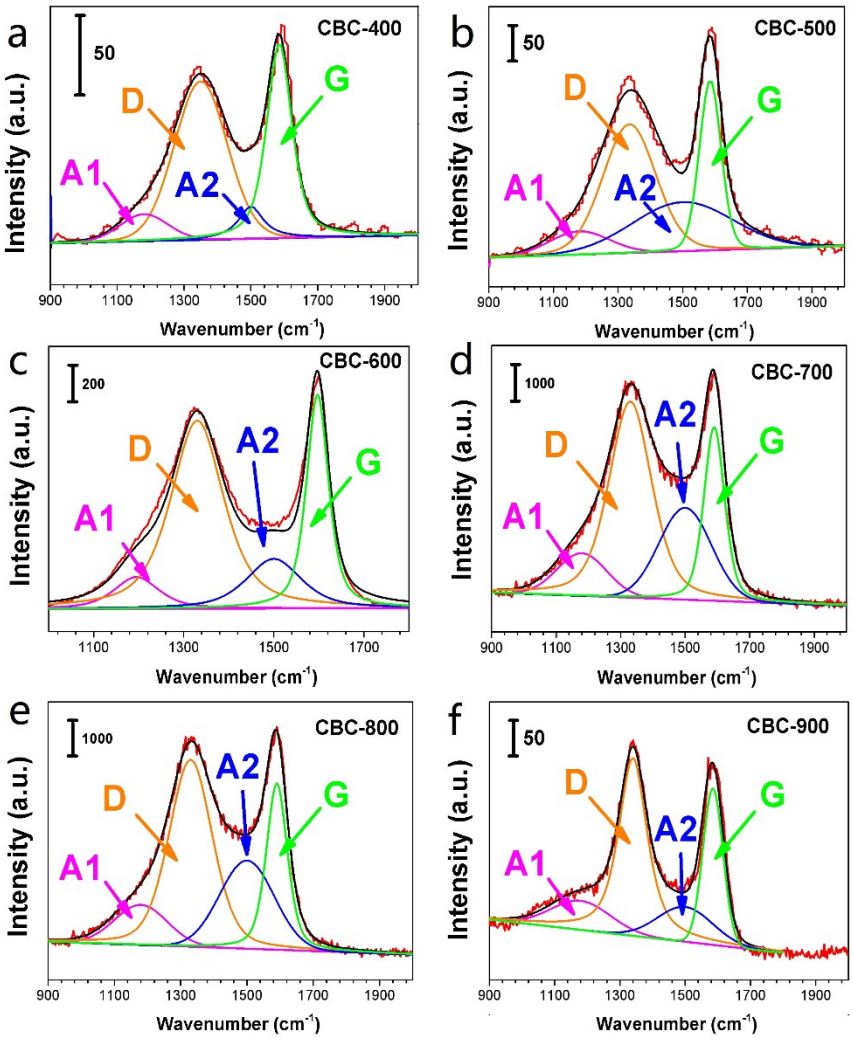

Figure S6. Raman spectra of CBC-T series products fitted with A1, D, A2 and G Gaussian peaks: (a) CBC-400, (b) CBC-500, (c) CBC-600, (d) CBC-700, (e) CBC-800 and (f) CBC-900.

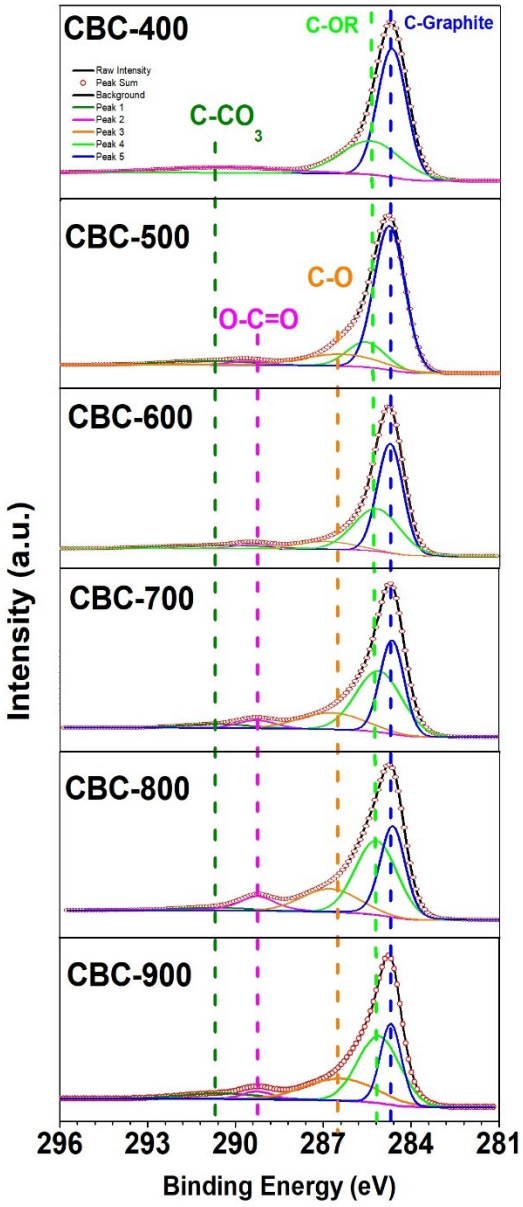

Figure S7. XPS survey corresponding high-resolution spectra of C elements of CBC-T.

SI.7 The calculation details of XANES

The CK-edge jump at ionization potential was fitted using an error function multiplied by an exponential decay function described by the following equation[1] :

$$I_{step} = H\left\{0.5 + 0.5erf\left[\frac{(E - P)}{W/C}\right]\right\} * \exp\left\{ - \left[d(E - P - W)\right]\right\}, E > P + W$$

Where H is the height of the function immediately above the step, E is the independent variable energy, P is the position of the inflection point of the step, W is the full width at half maximum of the step, d is the exponential decay coefficient, and C is the constant. The resulting spectrum was then fitted using multiple Gaussian peaks.[2]

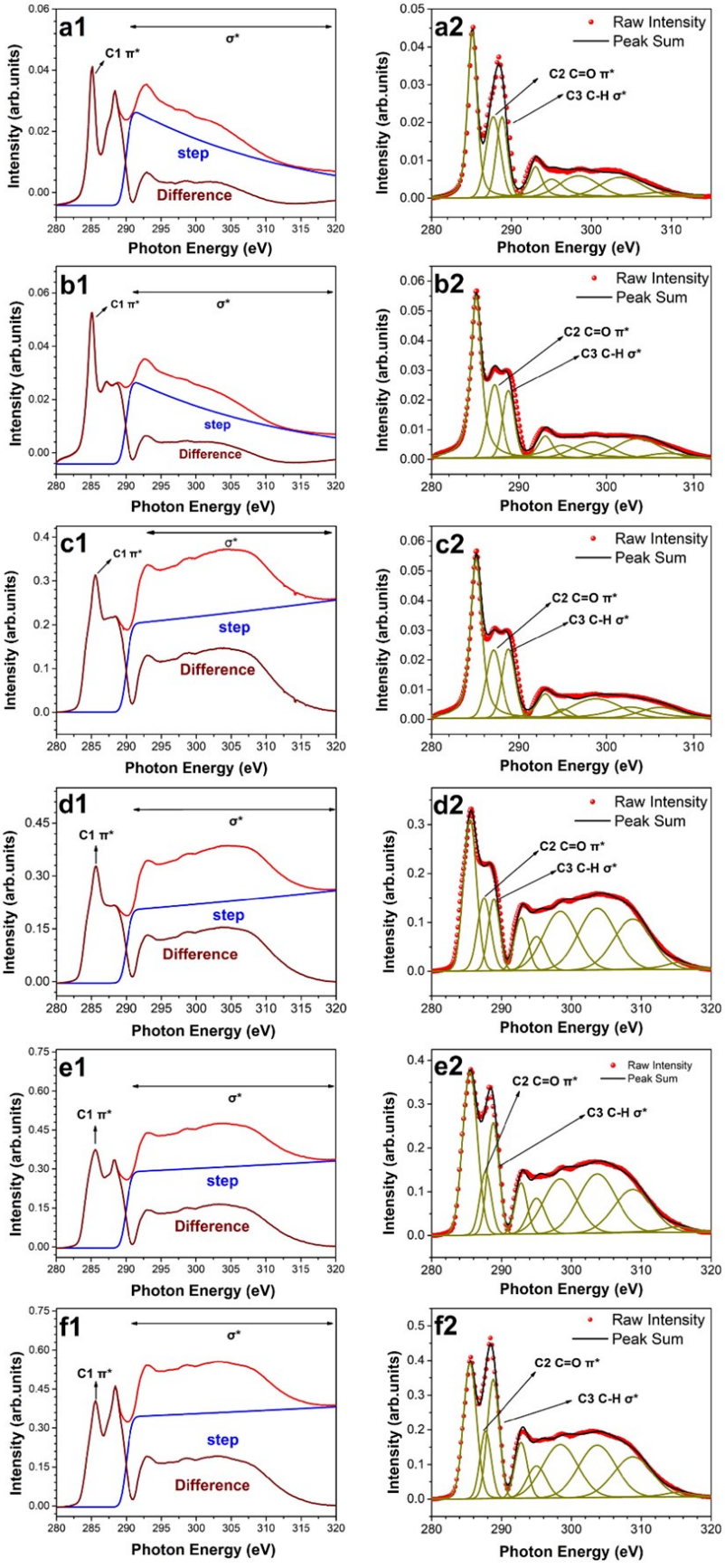

Figure S8. Deconvolution of XANES spectra of (a1&a2) CBC-400; (b1&b2) CBC-500; (c1&c2) CBC-600; (d1&d2) CBC-700; (e1&e2) CBC-800; (f1&f2) CBC-900.

SI.8 The UV-Vis image of CBC-T

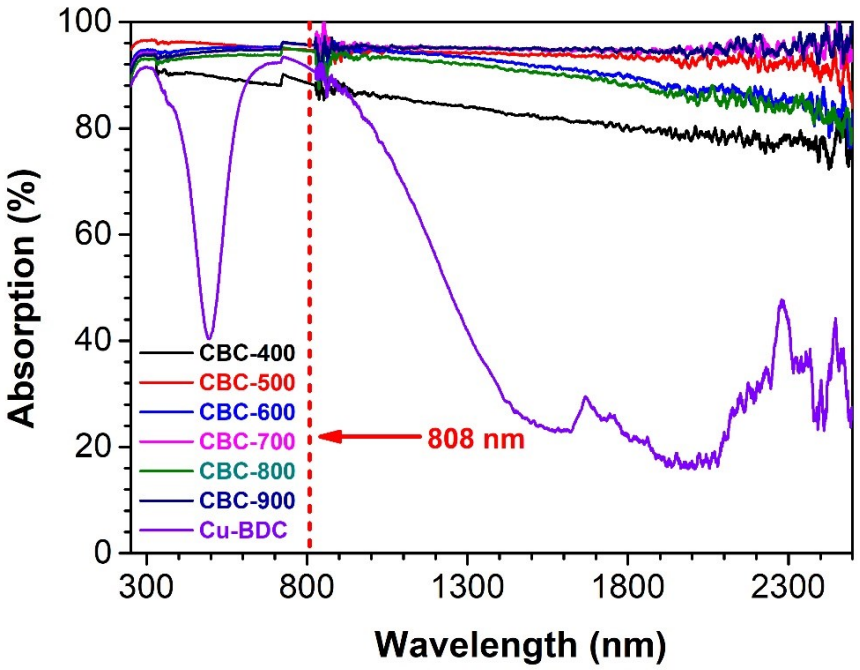

Figure S9. The Absorption image of CBC-T and Cu-BDC.

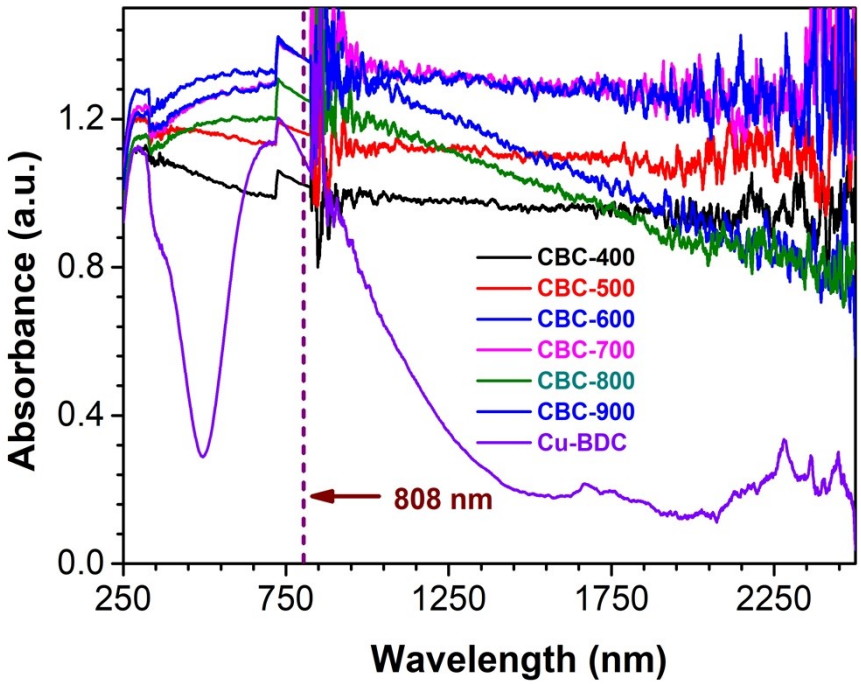

Figure S10. The Absorbance image of CBC-T and Cu-BDC.

SI.9 Calculation of photothermal conversion efficiency of CBC-T

The photothermal conversion efficiency was determined according to previous method.[8,16,17,29] Details are as follows:

Based on the total energy balance for this system:

$$\sum_i m_i C_{pi} \frac{dT}{dt} = Q_s - Q_{loss}$$

where m_i (0.35 g) and $C_{p,i}$ (0.8 J (g $^oC)^{-1}$) are the mass and heat capacity of system components (Cu-BDC and CBC-T samples and quartz glass), respectively. Q_s is the photothermal heat energy input by irradiating NIR laser to the samples, and Q_{loss} is thermal energy lost to the surroundings. When the temperature is maximum, the system is in balance:

$$Q_s = Q_{loss} = hS \Delta T_{max}$$

where h is heat transfer coefficient, S is the surface area of the container, ΔT_{max} is the maximum temperature change. The photothermal conversion efficiency η is calculated from the following eaquation:

$$\eta = \frac{hS \Delta T_{max}}{I(1 - 10^{-A_{808}})}$$

where I is the laser power (0.8 W cm^{-2}) and A_{808} is the absorbance of the samples at the wavelength of 808 nm (as showed in Figure S5).

In order to obtain the hS, a dimensionless driving force temperature, θ is introduced as follows:

$$\theta = \frac{T - T_{surr}}{T_{surr}^{max}}$$

where T is the temperature of the sample, T_{max} is the maximum system temperature, and T_{surr} is the initial temperature (about 33 ^oC).

The sample system time constant τ_s

$$\tau_s = \frac{\sum_i m_i C_{pi}}{hS}$$

thus $$\frac{d\theta}{dt} = \frac{1}{\tau_s} \frac{Q_s}{hS \Delta T_{max}} \frac{\theta}{\tau_s}$$

when the laser is off, $Q_s = 0$, therefore $\frac{d\theta}{dt} = -\frac{\theta}{\tau_s}$, and $t = -\tau_s \ln \theta$

so hS could be calculated from the slope of cooling time vs lnθ. Therefore, τ_s is about 280s.

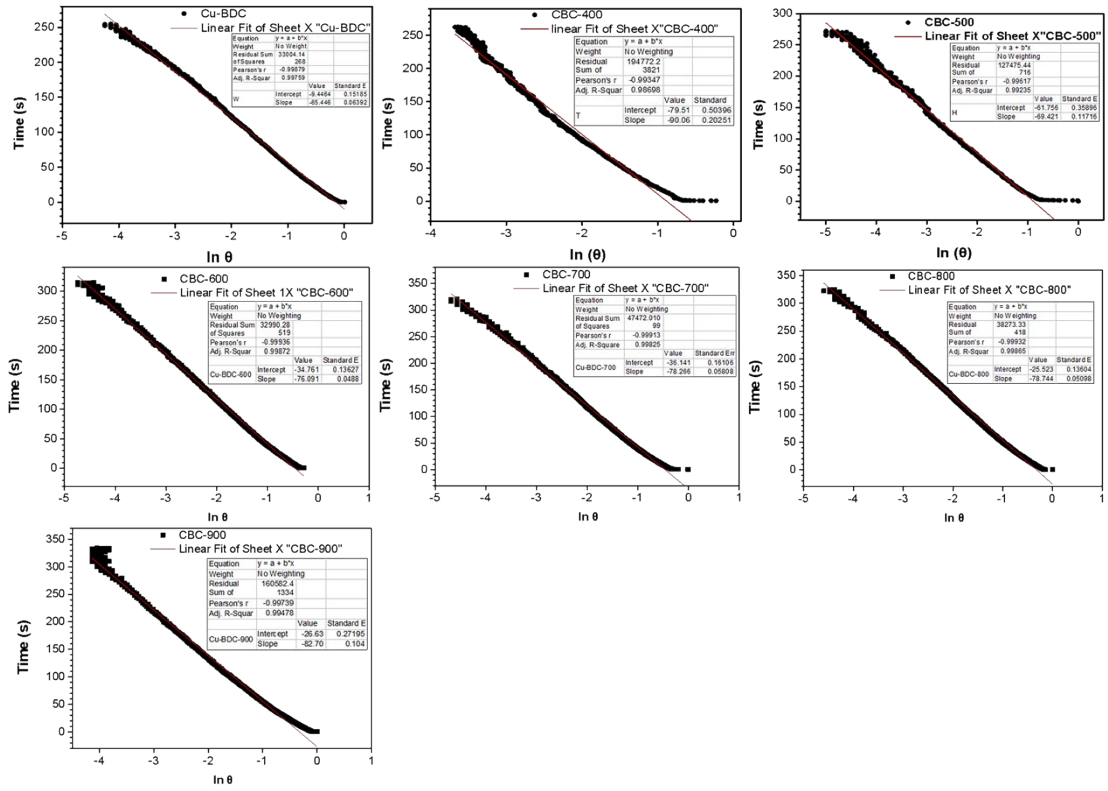

Figure S11. corresponding time-ln θ linear curve of CBC-T.

Table S2. Comparison of the photothermal efficiency (η) among CBC-T.

sample	Max temperature difference (℃)	η (%)
Cu-BDC	62	36.34
CBC-400	110	48.31
CBC-500	118	64.42
CBC-600	91	43.78
CBC-700	86	40.31
CBC-800	78	36.62
CBC-900	67	29.51

Table S3. Photothermal conversion efficiency with different concentrations.

Contrast Sample	η (%)	Classification	Ref.
CNT	44.8	carbon	3
Carbon Nanospheres	46.3	carbon	4
Carbon dots	43.9	carbon	5
Graphene Quantum Dots	87.9	carbon	6
Porous Carbon	48.5	carbon	7

CBC-500	64.42	carbon	Our Work
Perylenediimide-MOF	52.3	complex	8
Quaterrylenediimide	62.4	organic	9
nanoparticles	54.9	organic	10
perylene bisimide	59.5	organic	11
Dopamine-Melanin Colloidal Nanosphere	40	organic	12
Nanofibers	22.36	organic	13
Perylene diimide	31.6	organic	14
Terrylenediimide-Based material	41	organic	15
Organic cocrystal	18.8	organic	16
Poly(3,4-ethylenedioxyselenophene)	42.5	polymer	17
polymer nanoparticles	50	polymer	18
MOF	21.6	inorganic	19
MOF	33	inorganic	20
Chalcogenide	35	inorganic	21
Copper Selenide Nanocrystals	22	inorganic	22
gold nanoshells	13	metal	22
gold nanorods	21	metal	22
Cu_9S_5	25.7	Metal composite	23
Cu_7S_4 Nanosuperlattices	65.7	Metal composite	24
$Cu_{7.2}S_4$ nanocrystals	56.7	Metal composite	25
Bi_2S_3 -Au	51.6	Metal composite	26
Au−Cu_9S_5	37	Metal composite	27
$W_{18}O_{49}$	59.6	Metal oxide	28

SI.10 The SEM image of evaporator devices

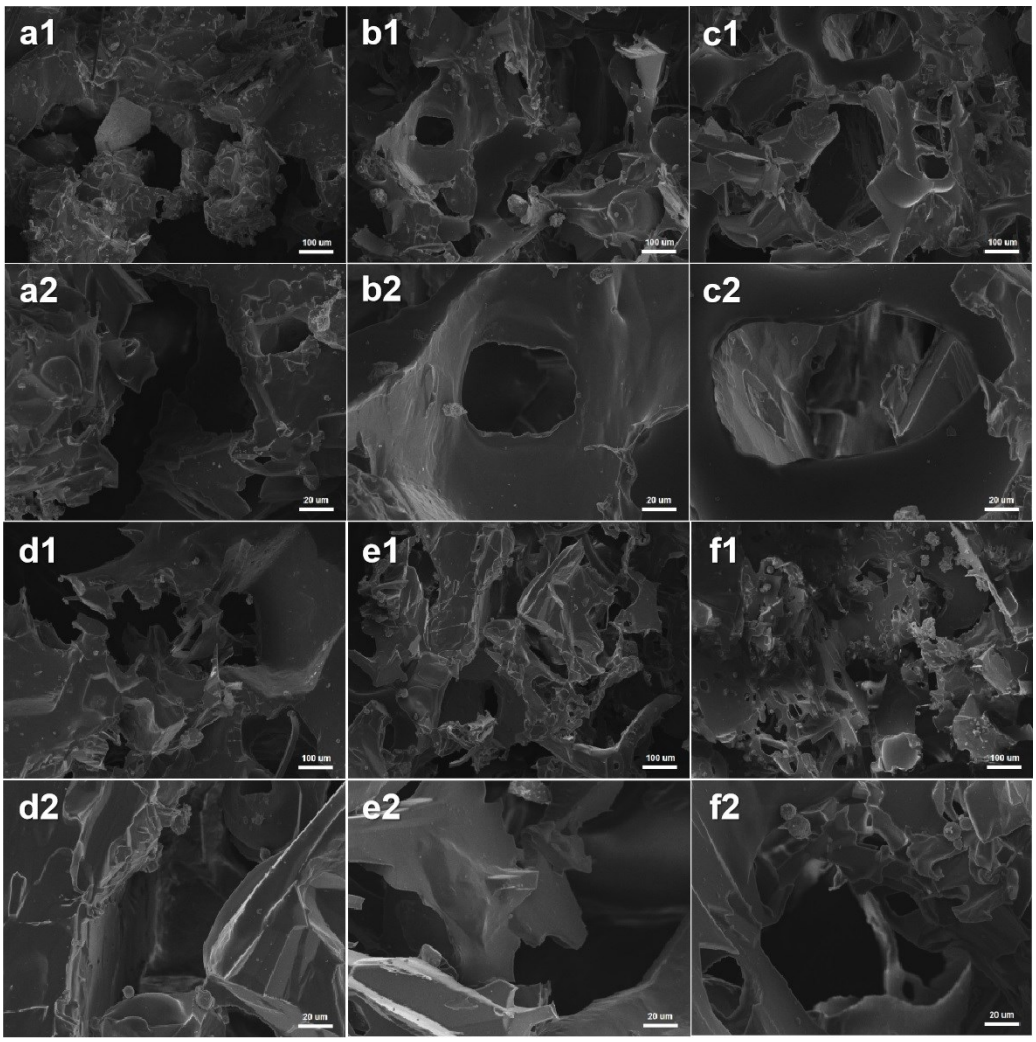

Figure S12. SEM image of (a) pure PDMS, (b) CBC-500-0.1%, (c) CBC-500-0.2%,(d) CBC-500-0.5%, (e) CBC-500-0.1% and (f) CBC-500-0.1%.

SI.11 The analysis of heat loss:

Heat loss to the environment includes three parts: (i)heat radiation to air, (ii)heat convection to air and (iii)heat conduction to water. The heat loss is calculated as follow:

Radiation:

The radiation loss was calculated using the Stefan-Boltzmann equation：

$\varphi=\varepsilon A\sigma(T4\ 1-T4\ 2)$

where φ represents heat flux, ε is the emissivity, and emissivity in this equation is supposed has a maximum emissivity of 1. A is the surface area (m^2), σ is the StefanBoltzmann constant (5.67×10^{-8} W m^{-2} K^{-4}), T_1 is the surface temperature (37℃) of heterostructured membrane-based absorber at a steady state condition, and T_2 is the ambient temperature (27℃) upward the absorber. According to the equation, the radiation heat loss is calculated 6%.

Convection:

The convective heat loss is defined by Newton' law of cooling:

$Q = hA\Delta T$

where Q represents the heat energy, h is the convection heat transfer coefficient (1 W m^{-2} K), and ΔT (10 ℃) is different value between the surface temperature of heterostructured membrane-based absorber and the ambient temperature upward the absorber. According to the equation, the connection heat loss is measured 4%.

Conduction:

$Q = Cm\Delta T$

where Q is the heat energy, C is the specific heat capacity of water (4.2 kJ $℃^{-1}$ kg^{-1}), m (50 g) is the weight of pure water used in this experiment. ΔT is the temperature difference of pure water after and before solar illumination under 1 sun after 1 h (0.5 ℃). The conduction loss was calculated about 7%.

SI.12 The analysis of contact angle

The contact angle measurement was tested by KRUSS DSA 100.

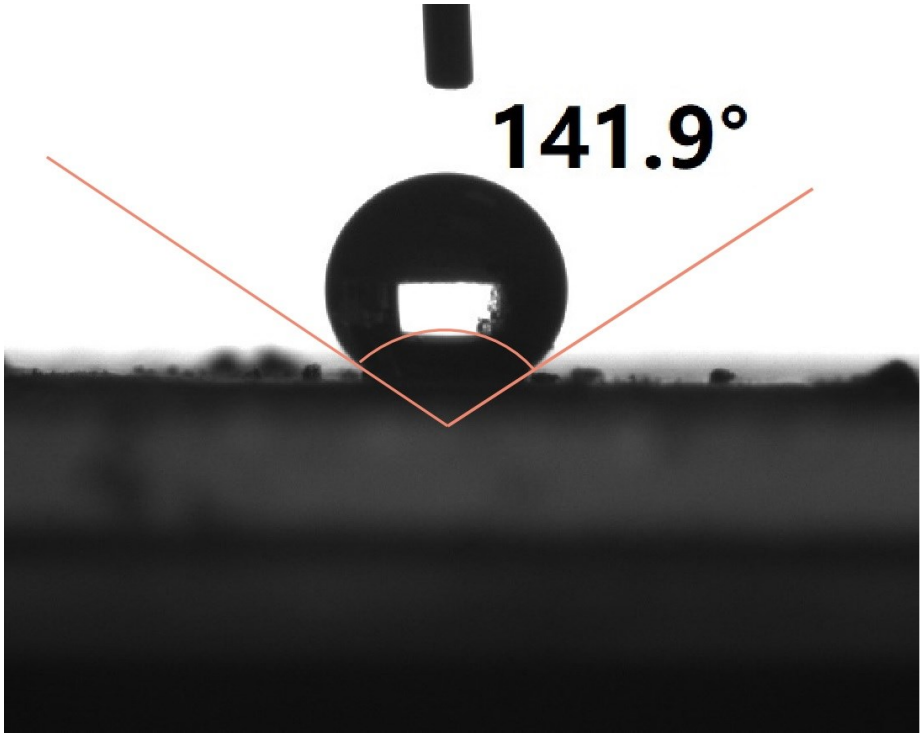

Figure S13. Surface wetting property of CBC-500.

SI.13 The analysis of recycle test

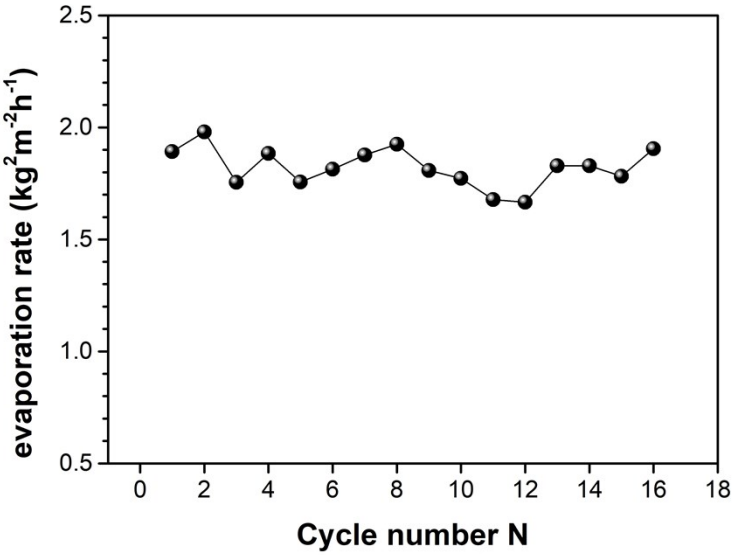

Figure S14. The stability of the evaporator under 1 sun illumination over sixteen cycles of evaporation.

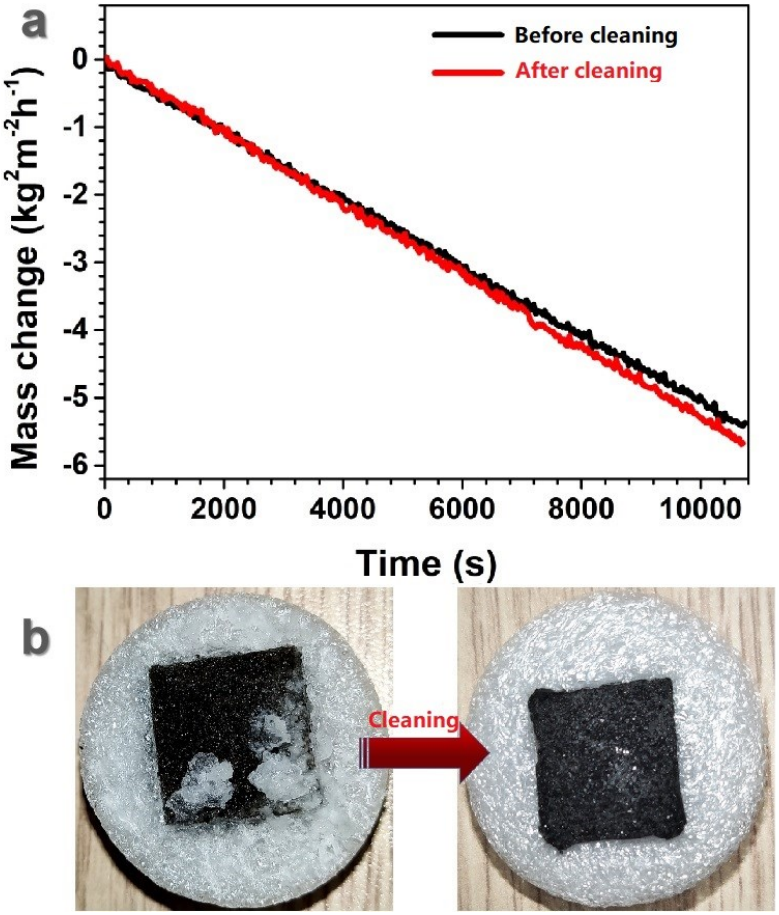

Figure S15. (a) The rate of evaporation before and after the evaporator is washed. (b) surface solid accumulation after the seawater evaporation and the evaporator after the salt removal by hand washing.

SI.14 The Stability of samples before and after illumination

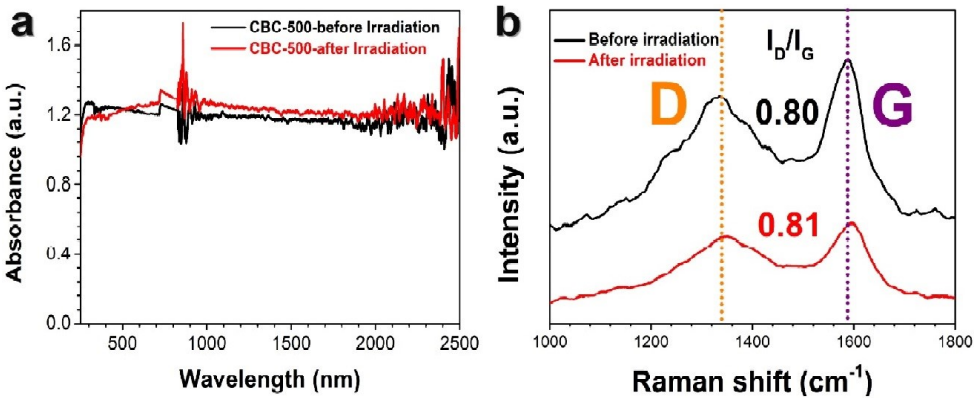

Figure S16. (a) The absorbance value of the CBC-500 changes before and after sunlight irradiation. (b) The Raman spectrum of the sample changes before and after sunlight irradiation.

Reference

1 N. Soin, S.S. Roy, S.C. Ray, P. Lemoine, M.A. Rahman, P.D. Maguire, S.K. Mitra, J.A. McLaughlin, Thin Solid Films, 2012, 520, 2909-2915.

2 R. Gago, I. Jiménez, J.M. Albella, Surf. Sci., 2001, 482, 530-536.

3 X. Du, J. Xu, S. Deng, Z. Du, X. Cheng, H. Wang, ACS Sustain. Chem. Eng., 2019, 7, 17682-17690.

4 L. Zhou, Y. Jing, Y. Liu, Z. Liu, D. Gao, H. Chen, W. Song, T. Wang, X. Fang, W. Qin, Z. Yuan, S. Dai, Z.-A. Qiao, C. Wu, Theranostics, 2018, 8, 663-675.

5 W. Su, H. Wu, H. Xu, Y. Zhang, Y. Li, X. Li, L. Fan, Mater. Chem. Front., 2020, 4, 821-836.

6 S. Li, S. Zhou, Y. Li, X. Li, J. Zhu, L. Fan, S. Yang, ACS Appl. Mater. Interfaces, 2017, 9, 22332-22341.

7 Y. Weng, S. Guan, L. Wang, H. Lu, X. Meng, G.I.N. Waterhouse, S. Zhou, Small, 2020, 16, 1905184.

8 B. Lü, Y. Chen, P. Li, B. Wang, K. Müllen, M. Yin, Nat. Commun., 2019, 10, 767.

9 C. Liu, S. Zhang, J. Li, J. Wei, K. Müllen, M. Yin, A Water-Soluble, Angew. Chem. Int. Ed., 2019, 58, 1638-1642.

10 Z. Zhao, C. Chen, W. Wu, F. Wang, L. Du, X. Zhang, Y. Xiong, X. He, Y. Cai, R.T.K. Kwok, J.W.Y. Lam, X. Gao, P. Sun, D.L. Phillips, D. Ding, B.Z. Tang, Nat. Commun., 2019, 10, 768.

11 L. Cui, Y. Jiao, A. Wang, L. Zhao, Q. Dong, X. Yan, S. Bai, Chem. Commun., 2018, 54, 2208-2211.

12 Y. Liu, K. Ai, J. Liu, M. Deng, Y. He, L. Lu, Adv. Mater., 2013, 25, 1353-1359.

13 Y. Jiao, K. Liu, G. Wang, Y. Wang, X. Zhang, Chem. Sci., 2015, 6, 3975-3980.

14 S. Zhang, W. Guo, J. Wei, C. Li, X.-J. Liang, M. Yin, ACS Nano, 2017, 11, 3797-3805.

15 Y. Wang, W. Zhu, W. Du, X. Liu, X. Zhang, H. Dong, W. Hu, Angew. Chem. Int. Ed., 2018, 57, 3963-3967.

16 B. Kim, H. Shin, T. Park, H. Lim, E. Kim, Adv. Mater., 2013, 25, 5483-5489.

17 H. Chen, J. Zhang, K. Chang, X. Men, X. Fang, L. Zhou, D. Li, D. Gao, S. Yin, X. Zhang, Z. Yuan, C. Wu, Biomaterials, 2017, 144, 42-52.
18 W. Wang, L. Wang, Y. Li, S. Liu, Z. Xie, X. Jing, Adv. Mater., 2016, 28, 9320-9325.
19 S. Wang, L. Shang, L. Li, Y. Yu, C. Chi, K. Wang, J. Zhang, R. Shi, H. Shen, G. I. N. Waterhouse, S. Liu, J. Tian, T. Zhang, H. Liu, Adv. Mater., 2016, 28, 8379-8387.
20 H. Zhu, Z. Lai, Y. Fang, X. Zhen, C. Tan, X. Qi, D. Ding, P. Chen, H. Zhang, K. Pu, Small, 2017, 13, 1604139.
21 C.M. Hessel, V.P. Pattani, M. Rasch, M.G. Panthani, B. Koo, J.W. Tunnell, B.A. Korgel, Nano Lett., 2011, 11, 2560-2566.
22 Q. Tian, F. Jiang, R. Zou, Q. Liu, Z. Chen, M. Zhu, S. Yang, J. Wang, J. Wang, J. Hu, ACS Nano, 2011, 5, 9761-9771.
23 J. Cui, R. Jiang, S. Xu, G. Hu, L. Wang, Small, 2015, 11, 4183-4190.
24 B. Li, Q. Wang, R. Zou, X. Liu, K. Xu, W. Li, J. Hu, Nanoscale, 2014, 6, 3274-3282.
25 Y. Cheng, Y. Chang, Y. Feng, H. Jian, Z. Tang, H. Zhang, Angew. Chem. Int. Ed., 2018, 57, 246-251.
26 X. Ding, C.H. Liow, M. Zhang, R. Huang, C. Li, H. Shen, M. Liu, Y. Zou, N. Gao, Z. Zhang, Y. Li, Q. Wang, S. Li, J. Jiang, J. Am. Chem. Soc., 2014, 136, 15684-15693.
27 Z. Fang, S. Jiao, Y. Kang, G. Pang, S. Feng, ChemistryOpen, 2017, 6, 261-265.